
Residual Contrastive Learning for Joint Demosaicking and Denoising

Nanqing Dong¹*, Matteo Maggioni², Yongxin Yang², Eduardo Pérez-Pellitero²,
Ales Leonardis², Steven McDonagh²

¹ Department of Computer Science, University of Oxford

² Huawei Noah's Ark Lab

Abstract

The breakthrough of contrastive learning (CL) has fueled the recent success of self-supervised learning (SSL) in high-level vision tasks on RGB images. However, CL is still ill-defined for low-level vision tasks, such as *joint demosaicking and denoising* (JDD), in the RAW domain. To bridge this methodological gap, we present a novel CL approach on RAW images, *residual contrastive learning* (RCL), which aims to learn meaningful representations for JDD. Our work is built on the assumption that noise contained in each RAW image is signal-dependent, thus two crops from the same RAW image should have more similar noise distribution than two crops from different RAW images. We use residuals as a discriminative feature and the *earth mover's distance* to measure the distribution divergence for the contrastive loss. To evaluate the proposed CL strategy, we simulate a series of unsupervised JDD experiments with large-scale data corrupted by synthetic signal-dependent noise, where we set a new benchmark for unsupervised JDD tasks with unknown (random) noise variance. Our empirical study not only validates that CL can be applied on distributions (*c.f.* features), but also exposes the lack of robustness of previous non-ML and SSL JDD methods when the statistics of the noise are unknown, thus providing some further insight into signal-dependent noise problems.

1 Introduction

The renaissance of contrastive learning (CL) [1] has made a significant impact on the development of self-supervised learning (SSL)² with large-scale unlabeled data. So far, progress in the vision domain mainly pertains to the area of high-level tasks [16, 29, 33, 4, 34], such as image recognition, object detection, and semantic/instance segmentation, which utilize instance discrimination as a pretext task to learn semantic visual representations. When it comes to low-level tasks, such as *joint demosaicking and denoising* (JDD) [19], which transforms noisy RAW images to clean RGB images, CL meets a challenge. Intuitively, demosaicking and denoising make less use of semantic information than high-level tasks in the learning phase. A second challenge with CL for JDD comes from the data domain. Unlike the RGB domain, where CL is well studied and instance-wise difference are formally defined, the RAW domain thus far lacks such investigation. Modern camera sensors capture only a single color at each photoreceptor. The camera color filter array (CFA) defines this capture pattern and results in a regular subsampling of red, green, blue color channels. Thus, each pixel of a captured RAW image contains only partial information necessary to reconstruct a full sample, and sensor measurement noise further corrupts captured data. Due to hardware limitations, noise may

*Work done as an intern at Huawei Noah's Ark Lab.

²In this work, we use the term self-supervised learning interchangeably with the term self-supervised representation learning for simplicity.

be introduced at different stages when transforming a photon to a digital pixel value. The noise is dependent on various factors such as scene and sensor, which makes the noise *signal-dependent* [10]. The nature of this physical image capture process makes JDD a challenging, ill-posed inverse problem, and also makes formulation of CL for JDD a hard problem.

In this work, we aim to answer an underexplored question: how to formulate the instance discrimination task low-level vision problems in the RAW domain. Specifically, instead of applying the contrastive loss on RAW images directly, we approach this question by examining the noise contained in the RAW images. We conjecture that this signal-dependent characteristic of noise in RAW images could be potentially used as a discrimination feature for CL. Yet, a key challenge stems from the fact that the contrastive loss [30] is mainly designed for semantic feature vectors. How to apply contrastive loss for noise distributions remains an open question.

We propose a CL framework which performs instance discrimination based on statistical distributions. In contrast to recent CL works [16, 29, 33, 4], we learn representations from the statistics of residuals instead of features, which we term *residual contrastive learning* (RCL). RCL for JDD consists of two components, a consistency loss and a *residual contrastive loss* (RCL³). The consistency loss aims to learn a coarse mapping from RAW to RGB by minimizing the distributional discrepancy between the original RAW crops and the reconstructed RAW crops, where the numerical difference are the *residuals*. We define each element of the proposed *residual statistics vector* (RSV) to be the sample mean of the residuals along certain axes of the residual tensors. We use an *earth mover’s distance* (EMD) to measure the similarity between two residual statistics vectors. Under signal-dependent noise, we assume that the RSVs of two crops extracted from the same RAW image have smaller distance than the RSVs of two crops extracted from two different RAW images. We enforce this assumption by minimizing InfoNCE [30] on RSVs. At this point, we have answered the posed question by proposing RCL which integrates residual learning [17] and CL.

To validate our assumption and to evaluate this new learning strategy, we perform the first, to the best of our knowledge, empirical study on simulated JDD tasks with unknown variance of noise. We note that, for statistical efficiency, previous non-ML [32] and SSL methods make an *i.i.d* Gaussian assumption with fixed standard deviation σ over the synthetic noise and σ is either known or can be estimated easily. Collection and curation of large-scale RAW images in a controllable environment, towards quantitative analysis of RCL with real data poses a task of high value and yet also high expense. Instead, we firstly use large-scale Monte-Carlo experiments to simulate signal-dependent noise. We assign each RAW image, generated by a reverse Image Signal Processor (ISP) pipeline [12], a unique σ to generate the synthetic noise. Note, the quality of learned representations is difficult to assess directly [16, 29, 33, 4]. Concretely, we use a self-supervised JDD method *mosaic2mosaic* [8] as the baseline model and incorporate our RCL as an additional module. In this way we use the performance of JDD tasks as a *proxy* measure; RCL should improve the performance of the baseline if it is learning truly useful representations from residuals. The experiments can be decomposed into two parts. In the first part, we set up a simulated model for the signal-dependent noise for all experiments. We extensively compare RCL with seminal non-ML and SSL methods for a thorough empirical understanding of JDD with unknown σ and a quantitative evaluation of RCL on large-scale datasets. Two major observations are (1) previous non-ML and SSL methods can not address this theoretical scenario of unknown σ , and (2) RCL does improve the baseline by a large margin (*e.g.* $>+8$ dB on average in our experiments). In the second part, we further analyze the properties and potential applications under various situations, including comparison with state-of-the-art (SOTA) methods on small-scale datasets, transferring the learned representations to unseen datasets, comparison with supervised learning (SL), and using RCL for unsupervised pre-training. Overall, the empirical findings in this work provide insights into a new research direction for JDD with signal-dependent noise.

Contributions Our contributions can be summarised as: (i) to the best of our knowledge, we are the first to formulate the instance discrimination task on RAW images for computational photography tasks; (ii) we propose a novel CL approach by learning representations from residuals; (iii) we demonstrate that InfoNCE can be applied on the distance between statistical distributions as a robust measurement; (iv) we provide insights into and empirically analyze the unknown σ problem in JDD

³In this work, we somewhat overload RCL to denote residual contrastive *learning* and residual contrastive *loss* interchangeably; residual contrastive learning essentially involves applying a residual contrastive loss, in our context.

tasks by simulating signal-dependent noise in a Monte-Carlo fashion; (v) we evaluate RCL for JDD tasks and set a new SOTA for the unsupervised JDD problem with unknown σ .

2 Background

RAW Image Noise Model The process of transforming photons recorded from the scene into quantized digital values consists in a sequential pipeline of complex operations applied to the sensed data. The acquisition is subject to various factors such as dark current, exposure time, sensor saturation, and gain factor. Further, noise may be introduced at different stages due to hardware limitations. The noise is usually modelled as a zero-mean random variable with variance depending on the underlying (unknown) signal as well as the camera acquisition settings [10, 15, 21, 12]. Conventionally, the variance σ^2 of the noise r.v. n is defined as

$$\sigma_n^2 = \frac{\Phi t}{g^2} + \frac{\sigma_{\text{read}}^2}{g^2} + \sigma_{\text{ADC}}^2. \quad (1)$$

The first term denotes the photon noise, where Φ is the radiant power, t is the exposure time, and g is the sensor gain. The terms σ_{read}^2 and σ_{ADC}^2 are the variance of the readout noise and the variance of the analog-to-digital conversion (ADC) noise [15], respectively. From Eq. 1, we know that the noise in a RAW image is related to both the sensor input and the environment with which the sensor input interacts, as well as the camera settings. That is to say, σ_n^2 is signal-dependent.

Contrastive Learning CL was first developed as a learning paradigm for neural networks in order to identify what makes two objects similar or different [1]. Recent studies on self-supervised representation learning [4, 16, 29, 33] extend this idea by connecting contrastive loss with an instance discrimination *pretext* task. One widely used contrastive loss, InfoNCE [30], is formulated as,

$$\mathcal{L}_{\text{NCE}} = -\log \frac{\exp(\text{sim}(z_q, z_0)/\tau)}{\sum_{i=0}^N \exp(\text{sim}(z_q, z_i)/\tau)} \quad (2)$$

where z is the feature vector extracted from an image patch of interest, τ is a temperature parameter and $\text{sim}(\cdot, \cdot)$ is the cosine similarity function. For image classification tasks, it is common to use a CNN backbone (*e.g.* ResNet [17]) as the feature extractor, encoding images into feature vectors. Then, $\text{sim}(\cdot, \cdot)$ can be used to measure the similarity between feature vectors. Here, (z_q, z_0) is a positive pair, where two patches are taken from the same image; and $(z_q, z_{i>0})$ is a negative pair, where two patches are taken from different images. Loosely speaking, minimizing Eq. 2 encourages the networks to learn features that are invariant between two visually similar instances, to the benefit of downstream tasks. As proven in [5], large N is required for reasonable performance. For representation learning, CL approaches have mainly been designed for, and focused on, classification tasks. The consideration of these topics in relation to low-level vision problems is understudied.

3 Problem Formulation

Let x be a noisy sensor signal in RAW format with additive noise n and clean sensor signal y , *i.e.* we have $x = y + n$. Following the previous discussion, n follows a distribution with a zero mean and a variance depending on the underlying but unknown y . For statistical efficiency [27, 25, 2, 24, 14, 35], it is common to approximate $n \sim \mathcal{N}(0, \sigma_n^2(y))$, *i.e.* n as a Gaussian distribution. Assume r is the corresponding reference RGB signal of x , which is treated as the ground truth (GT) for the JDD task.

For standard SL, we have training set $\mathcal{S} = \{(x_i, r_i)\}_{i=1}^{N_S}$, with N_S training examples. In this work, we assume N_S to be sufficiently large. Additionally, following Eq. 1, we assume the RAW images have signal-dependent noise. Let f_θ be a neural network that maps a RAW signal to RGB image, the objective is then to minimize $\sum_i \|f_\theta(x_i) - r_i\|$, where $\|\cdot\|$ is a distance metric (*e.g.* ℓ_1 norm or ℓ_2 norm). For SSL, the GT RGB images are unavailable during training and we have $\mathcal{S} = \{x_i\}_{i=1}^{N_S}$.

4 Residual Contrastive Learning for Joint Demosaicing and Denoising

In this section, we introduce our contribution *residual contrastive learning* (RCL) for JDD. We firstly describe the baseline self-supervised JDD model and will then discuss the motivation of this work and present the details of RCL. The overall framework of RCL is illustrated in Fig. 1.

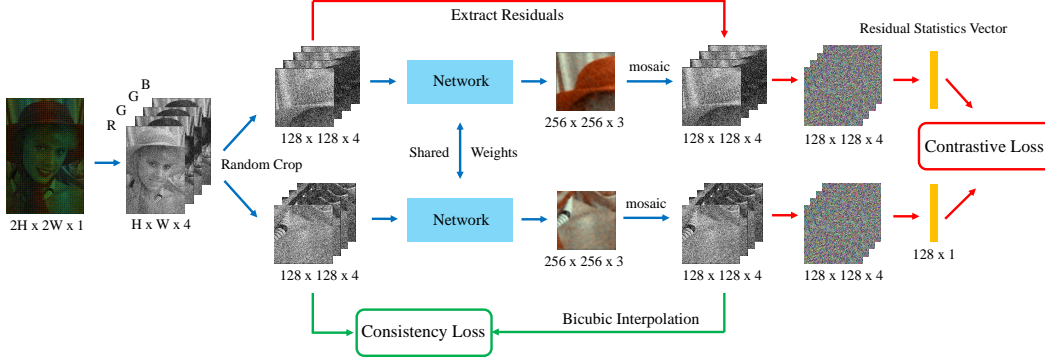


Figure 1: Illustration of RCL. The network maps a random crop from the RAW domain to the RGB domain. The model aims to minimize the distance between the mosaicked RGB crop and its original RAW counterpart via the consistency loss described in Sec. 4.1. Further, the contrastive loss (see Eq. 2) is minimized to discriminate whether two residual vectors are extracted from the same RAW image (a positive pair) or from two different RAW images (a negative pair), described in Sec. 4.3.

4.1 Consistency Loss

Motivated by [8], our backbone self-supervised JDD model is based on consistency training. We define the consistency loss as a reconstruction loss

$$\mathcal{L}_{\text{consistency}} = \|\text{mosaic}(\mathcal{T}(f_{\theta}(x))) - x\|, \quad (3)$$

where $\text{mosaic}(\cdot)$ is a standard image mosaic operation, which only samples one color per pixel, and $\mathcal{T}(\cdot)$ is bicubic interpolation [20]. If x is a tensor of shape $H \times W \times 4$ (with the third dimension representing four colour channels; red, green, blue, green), then $f_{\theta}(x)$ is of shape $2H \times 2W \times 3$, and $\text{mosaic}(\mathcal{T}(f_{\theta}(x)))$ will retain shape⁴ $H \times W \times 4$.

4.2 Motivation

Recent non-ML JDD approaches [11, 18, 32] typically assume standard *i.i.d* Gaussian noise with signal-independent variance, *i.e.* $n_i \sim \mathcal{N}(0, \sigma^2) \quad \forall x_i \in \mathcal{S}$. Although these methods have achieved promising results in practical situations without GT, this synthetic noise model ignores the fact that noise can be signal-dependent as in Eq. 1. There lacks an empirical understanding of the behaviors of recent non-ML or unsupervised JDD methods on data with signal-dependent noise.

From the perspective of representation learning, recent CL frameworks [30, 16, 4, 33, 29] design pretext tasks by utilizing the invariance between different views of the same instance, *i.e.* different crops of the same instance should contain similar semantic information. Mathematically, minimizing InfoNCE (Eq. 2) is equivalent to maximizing the mutual information of two views of the same image [30]. By minimizing InfoNCE the model is expected to learn invariant features, shared by pairs of views, in a SSL fashion [29, 4, 33]. Inspired by this line of research and the task under consideration, we assume that the noise distribution can help to distinguish positive and negative pairs for RAW images, thus we select to construct a contrastive loss on the relevant noise distributions.

4.3 Residual Contrastive Loss

We propose to utilize the concept of contrastive learning in JDD. For dense prediction tasks, Eq. 2 can be considered inappropriate as the prediction is not a feature vector and learning semantic information is likely of less direct help for dense prediction tasks such as JDD. Instead, we modify Eq. 2 and propose a new *residual contrastive loss* (RCL) for JDD. We first make the following assumption:

Assumption 1. *Two crops from the same instance have similar noise distributions and two crops from two different instances have two different noise distributions if $n \sim \mathcal{N}(0, \sigma^2(y))$.*

⁴If x is a tensor of shape $2H \times 2W \times 1$ in Bayer pattern, we can either easily transform it to $H \times W \times 4$ or just adapt f_{θ} to output $2H \times 2W \times 3$.

Assumption 1 constitutes a natural extension of the assumption that $n \sim \mathcal{N}(0, \sigma^2(y))$, following Eq. 1. In fact, for natural images, the last two terms in Eq. 1 for two crops from the same image should be identical and the first term could be correlated because of the potential self-similarity within the same image. A more accurate refinement is that two crops from the same instance should have detectably smaller divergence in noise distributions than two crops from two different instances.

We define the estimated residual tensor for x as $\hat{n}(x) = x - \text{mosaic}(f_\theta(x))$. Deep residual learning [17] has shown success in related supervised demosaicing tasks [21, 23]. In contrast to these supervised settings, we apply a contrastive loss on the residuals to fine-tune f_θ . Given the residual tensor \hat{n} with shape $H \times W \times 4$ elements. Let $\hat{n}_{i,j,k}$ denote the residual value at the i^{th} row, j^{th} column, and k^{th} channel of \hat{n} . We use the same notation z in Eq. 2 to denote a *residual statistics vector* (RSV), where we use a vector of sample mean residuals along certain axes to represent the sample residual distribution. Concretely, for the i^{th} element of a H -element, column-wise vector z , we have $z^i = \frac{1}{W \times 4} \sum_{j,k} \hat{n}_{i,j,k}$. Similarly we could use a W -element, row-wise vector. Intuitively, we are estimating the statistics of the residual distributions using the *Central Limit Theorem* (CLT) and the *Law of Large Numbers*. The sample mean offers a simple estimator, amenable to backpropagation and is also empirically found to be adequately discriminative. Thus, to better estimate basic statistics of the residual distribution, we require that H and W should not be small. Due to the CLT, the samples of the RSV should form a Gaussian distribution. We reformulate \mathcal{L}_{NCE} as

$$\mathcal{L}_{\text{contrast}} = -\log \frac{\exp(-d(z_q, z_0)/\tau)}{\sum_{i=0}^N \exp(-d(z_q, z_i)/\tau)}, \quad (4)$$

where τ is a temperature parameter [4] and $d(\cdot, \cdot)$ is a non-negative distance metric which measures the divergence between two probability distributions, such that larger $d(\cdot, \cdot)$ values indicate larger divergence. Note that, unlike cosine similarity, $d(\cdot, \cdot)$ should not assume a pair-wise relationship between two samples, as the noise distribution is independent of the pixel location. The $d(\cdot, \cdot)$ metric should also possess desirable properties such as ease of computation and differentiability, towards enabling efficient end-to-end training. In this work, we use the *earth mover's distance* (EMD) for $d(\cdot, \cdot)$, which makes no assumption over the data. The implementation of EMD for the 1D case is simple as it involves sorting operations, as shown in our Fig. 2 pseudocode. The final training objective is then the sum of the two introduced losses:

$$\mathcal{L}_{\text{total}} = \mathcal{L}_{\text{consistency}} + \lambda \mathcal{L}_{\text{contrast}}, \quad (5)$$

where λ is a weighting parameter chosen empirically to balance the contribution of $\mathcal{L}_{\text{consistency}}$ and $\mathcal{L}_{\text{contrast}}$ and align their order of magnitude.

As an aside, we note that $\text{sim}(\cdot, \cdot)$ in Eq. 2 (or $-d(\cdot, \cdot)$ in Eq. 4) can alternatively be learned in an adversarial fashion [13]. However, in practice we found no performance gain by introducing an auxiliary neural network to the optimization (see Sec. 5.1 for detail).

5 Experiments

5.1 Empirical Study on Images with Unknown Noise Distributions

Simulation We are the first to present a study towards empirical understanding of JDD on large-scale data, with simulated signal-dependent noise. We assume that RAW images are captured by different sensors independently and are collected from different scenes, towards incurring signal-dependent noise, as we previously formalize in Eq. 1. To simulate such signal-dependent noise, we employ a Monte-Carlo method to generate synthetic Gaussian noise ($\mathcal{N}(0, \sigma^2)$), where σ is randomly sampled from a uniform distribution $\mathcal{U}(0, 20)$. In this way, we consider each RAW image to have an approximately *unique* noise distribution. In fact, the synthetic noise generated by this process is still signal-independent noise, as σ is fixed for a given image. But from the perspective of the dataset \mathcal{S} , there is an approximate one-to-one mapping between σ and a RAW image. Thus, we consider each RAW image to have signal-dependent noise for the following experimental work. We use this simulation model as it is easy to evaluate the available methods in the literature as most of them are originally designed for *i.i.d* Gaussian noise.

```
# noise is estimated noise tensor
z1, _ = torch.mean(noise1, (1, 2)).sort()
z2, _ = torch.mean(noise2, (1, 2)).sort()
EMD = torch.mean(torch.abs(z1 - z2))
```

Figure 2: PyTorch implementation for EMD.

Implementation Theoretically, f_θ can be any CNN, designed for dense prediction tasks. To illustrate this point our first experiment utilizes U-Net [31] as the network backbone and we fix the random seed. To instantiate Eq. 4, we follow [4] in defining temperature τ values and use a batch size of 64. We use an ℓ_1 norm for Eq. 3 and weighting parameter $\lambda = 0.001$. We use the Adam [22] optimizer with $\beta_1 = 0.9$, $\beta_2 = 0.999$, and $\epsilon = 10^{-7}$, and a fixed learning rate 10^{-3} . The models are implemented in PyTorch on a NVIDIA Tesla V100 GPU. For example, the minimal crop size used in this work is $128 \times 128 \times 4$. We use a minimal crop size of $128 \times 128 \times 4$ for RAW images with an RRGB mosaic pattern, thus a RSV has 128 elements and each element is the average of 512 values.

Datasets In order to simulate the large-scale unlabeled training data, we consider three large-scale public datasets, namely the MIT Demosaicing Dataset [12] (MIT), the Stanford Taskonomy Dataset [36] (Stanford), and the PASCAL VOC Dataset [9] (VOC). The three datasets contains different semantic information and image quality. MIT is a benchmark dataset for JDD, containing images that are collected from the web with large variety in terms of object categories and scenes. Each RGB image is up-sampled to 512×512 to have a higher resolution for RCL. The RGB images in Stanford constitute indoor scenes with fixed resolution 512×512 . VOC is an image collection of 20 semantic categories and the RGB images have various resolution. Each RGB image is up-sampled so the short side has a minimal length of 256. Limited by available resources, we select two subsets of MIT and Stanford, and VOC to validate our ideas. The MIT subset contains 11000 images⁵, including 10000 images in the training set and 1000 images in the test set. The Stanford subset contains 9464 images⁶, and we use 8464 images for training and 1000 images for testing. VOC contains 17125 images, including 16125 for training and 1000 for testing. Following previous work [18, 12, 32, 8], each RGB image is mosaiced to form a Bayer pattern RAW image and synthetic Gaussian noise ($\mathcal{N}(0, \sigma^2)$) is added.

Baselines We compare the proposed framework with both seminal non-ML and SSL methods. Baseline methods are grouped into four categories: the first category consists of demosaicing algorithms without denoising, which are *bilinear* [26] and *Contour Stencils* [11]. The second and third categories pertain to sequential approaches consisting of either first demosaicing and then denoising, or first denoising and then demosaicing pipelines, respectively. We adopt a non-ML denoising baseline BM3D [6] and a SSL denoising baseline with a U-Net backbone. The fourth category are SOTA JDD methods, including two non-ML baselines; FlexISP [18] and ADMM [32], and a SSL baseline *mosaic2mosaic* (M2M) [8]. We do not use any data augmentation for RCL but keep network backbone consistent for M2M and RCL. For non-ML methods that require a σ parameter as part of method input, without any prior knowledge, we use the expectation of $\mathcal{U}(0, 20)$, *i.e.* $\sigma = \mathbb{E}[\mathcal{U}] = 10$. The PSNR and SSIM between predicted and reference RGB images, for each method, are reported in Table 1.

Analysis Firstly, we observe that SSL methods outperform non-ML methods in all datasets. With signal-dependent noise, SOTA non-ML JDD methods, such as ADMM and FlexISP, become less effective and output low quality RGB images in terms of both PSNR and SSIM. A random (unknown) σ is clearly challenging for non-ML methods. This problem might be potentially mitigated by using additional strategies to estimate noise variance from the noisy input, which are likely to be overestimated, yet is beyond the scope of the current discussion. Secondly, as a modular component, RCL consistently outperforms M2M (*w/o* and *w/* augmentation) by a large margin, where RCL and M2M utilise the same network backbone. Without discriminative learning, M2M is likely able to catch the σ of seen examples, yet unable to generalize well to unseen examples. Third, based on the results in Table 1, we hypothesize that the performance of SSL methods is clearly data-dependent for this task. Note, MIT is more blurry than VOC in terms of image quality, and Stanford has quite similar scenes, in comparison with VOC. As SSL methods tend to achieve higher performance in MIT and Stanford, we conjecture that SSL methods, especially RCL, may potentially benefit from these two factors in practical applications.

Bhattacharyya Distance In addition to EMD, we consider another statistical distance, *Bhattacharyya* distance (BD) [3], as a baseline. Appealingly, if two sample distributions are Gaussian, the BD can be computed in closed-form. Although BD and EMD can both improve the performance of M2M, EMD is apparently a better option for RCL than BD. We believe this may be explained by the fact that residuals do not perfectly fit Gaussian distributions.

⁵<https://groups.csail.mit.edu/graphics/demosaicnet/dataset.html>

⁶<https://github.com/alexsax/taskonomy-sample-model-1>

Table 1: Empirical analysis for JDD methods on data with simulated signal-dependent noise. The σ is random (unknown) when we generate synthetic signal-dependent noise. An unknown σ poses new challenges to non-ML methods.

Method	MIT [12]		Stanford [36]		VOC [9]	
	PSNR	SSIM	PSNR	SSIM	PSNR	SSIM
Demosaicing						
Bilinear [26]	12.16	0.1110	12.06	0.0827	12.37	0.1283
Contour Stencils [11]	12.99	0.1307	12.24	0.0870	12.76	0.1890
Demosaicing + Denoising						
bilinear [26] + BM3D [6]	11.92	0.0923	12.49	0.0899	12.32	0.1441
Contour Stencils [11] + BM3D [6]	14.90	0.1987	14.87	0.1487	12.64	0.1714
Denoising + Demosaicing						
BM3D [6] + bilinear [26]	15.48	0.2398	13.06	0.0988	14.07	0.1826
BM3D [6] + Contour Stencils [11]	17.55	0.2571	13.83	0.1044	16.53	0.3070
noise2self [2] + bilinear [26]	12.51	0.1232	13.56	0.1190	12.65	0.1379
noise2self [2] + Contour Stencils [11]	12.57	0.1157	14.43	0.1130	14.67	0.2052
Joint Demosaicing & Denoising						
FlexISP [18]	15.24	0.1635	14.26	0.0940	14.04	0.1331
ADMM [32]	13.37	0.1441	11.84	0.0772	12.29	0.1328
M2M [8] (w/o aug)	17.95	0.3565	18.67	0.3211	16.88	0.2518
M2M [8] (w/ aug)	18.51	0.3822	19.78	0.4419	17.82	0.3206
Ours						
RCL (BD)	28.07	0.8814	25.93	0.8293	23.27	0.6742
ARCL	25.53	0.8022	25.53	0.7633	21.86	0.5826
RCL	28.26	0.8863	26.39	0.8355	23.69	0.6812

Adversarial Learning for RCL As an ablation study, we also briefly investigate adversarial learning for RCL (ARCL). We use an auxiliary network g_ϕ to replace $\text{sim}(\cdot, \cdot)$ in \mathcal{L}_{NCE} (Eq. 2). Network g_ϕ has the same architecture as a standard GAN discriminator [13]; a three-layer MLP with hidden node size 256. Network g_ϕ takes as input the concatenation of two RSVs. Functions f_θ and g_ϕ then constitute the two components participating in a standard GAN minimax game [13]. Given a training mini-batch, we first maximize \mathcal{L}_{NCE} with f_θ , fixed for five steps, then minimize $\mathcal{L}_{\text{consistency}} + \lambda \mathcal{L}_{\text{NCE}}$ with g_ϕ , fixed for one step. The same set of hyperparameters apply. As shown in Table 1, ARCL can achieve comparable performance with RCL using BD yet the performance is lower than RCL with EMD. Note that computations for BD and EMD are fairly simple and fast while ARCL introduces additional memory footprint with no performance gain. We hypothesize that, with a tailored design for g_ϕ (e.g. via neural architecture search [37]), there is still space for the performance of ARCL to be improved, which we leave to future work.

5.2 Ablation Studies

Comparison with State-of-The-Art Non-ML methods assume signal-independent noise for \mathcal{S} , however we attempt to perform further meaningful comparisons between RCL and SOTA JDD approaches. We use two public benchmark datasets; Kodak [28] and MSR [21]. We upsample MSR images ($\times 2$) in both height and width to meet the minimal resolution for RCL. We consider two scenarios: fixed σ and random σ . Following Sec. 5.1, the random σ is sampled from $\mathcal{U}(0, 20)$ and the fixed σ is set to 10. For SSL methods, we use DemosaicNet [12] as the network backbone and augment RAW images with a random affine transformation, following [8]. Towards fair comparison, the networks are realized with fixed random seed. The results are presented in Table 2. We note that the Kodak and MSR datasets may be considered small-scale, in contrast to those considered in the previous section. This poses a challenge for RCL and, moreover, a fixed σ violates Assumption 1. We observe that RCL still achieves performance competitive with the SOTA. If σ is known, we may simply use M2M ($\lambda = 0$) or non-ML methods. However, σ is usually unknown in practice. RCL can be seen to improve the performance of M2M and outperforms non-ML methods by a large margin, in

Table 2: PSNR results on Kodak and MSR datasets.

Method	Kodak [28]		MSR [21]	
	$\sigma = 10$	Random	$\sigma = 10$	Random
FlexISP [18]	28.63	15.33	28.89	13.36
ADMM [32]	29.47	13.07	29.89	12.22
M2M [8]	29.20	21.71	29.84	22.00
RCL	29.03	22.90	29.47	23.21

Table 3: PSNR results of transferring representations from source datasets (rows) to target datasets (columns).

Dataset	Kodak	MSR
MIT	24.12	28.26
Stanford	23.21	27.97
VOC	24.55	28.14

the latter scenario. According to Table 1, we can observe that M2M does not benefit from large-scale datasets and augmentation does not help for unseen images, when σ is unknown.

Transferable Representations We examine the transferability of the representations learned by RCL. We pre-train a U-Net on source datasets and then evaluate directly on a separate target dataset. Large-scale datasets MIT [12], Stanford [36], and VOC [9] define the source datasets and Kodak [28] and MSR [21] are then used as target datasets. We use random $\sigma \in \mathcal{U}(0, 20)$ to generate the simulated signal-dependent noise as before. The PSNR results are presented in Table 3. It can be observed that results improve over analogous test dataset results from Table 2. This suggests that representations learned by RCL are also transferable, and RCL benefits from large-scale training data. Representations learned from Stanford data provide somewhat lower results. This may be caused by the fact that the Stanford data contains comparatively similar scene content.

Comparison with Supervised Learning We train a U-Net in a supervised fashion using VOC data, with the **same** random seed and $\sigma \in \mathcal{U}(0, 20)$. We use η to denote the number of GT RGB images, available during supervised training. The supervised results are presented in Table 4 under the column *w/o Pre-Training*. We observe that SL methods still have considerable advantages over the non-ML or SSL methods (the first row in Table 4 denotes the highest performance that non-ML or SSL methods can achieve).

Unsupervised Pre-Training Following the comparison with SL, we pose the following questions: *can RCL help SL?* and *when can RCL help?* We first pre-train a U-Net on the entire training set with RCL in an unsupervised fashion, then fine-tune the pre-trained U-Net with η additional paired RGB training images, as above. See Table 4 for quantitative comparison between “without” and “with” pre-training (*w/o* and *w/*, respectively). Pre-training with RCL does improve the performance of standard SL. In cases where labelled data are expensive to collect or curate, such pre-training may be able to offer significant improvement (*e.g.* $>+1.5$ dB with only 10 labels). We can observe that improvement margins diminish as η grows and since we dictate that σ is unknown, both easy and hard examples will be presented.

Analysis on EMD To validate Assumption 1, we calculate the EMD between vectors of the noise statistics, extracted from positive pairs and from negative pairs, based on the synthetic noise model in Sec. 5.1. As shown in Fig. 3a, EMD distances between positive pairs and between negative pairs follow two different distributions. To make sure that RCL can learn such a difference, we extract the estimated noise by using a UNet trained on MIT with RCL. Given an anchor RAW image, we calculate the pair-wise difference for EMD between a negative pair; one crop from the anchor and the second from a different image, and the EMD between a positive pair; two crops from the same anchor. Given the same network, we record the differences before the training starts (*i.e.* the weights are randomly initialized) and after the loss converges. The density plot of the differences is shown in

Table 4: PSNR results of a U-Net trained and tested on VOC. We report GT RGB images η , available at training time. The first row reports our best-performing SSL method. Column “*w/o Pre-Training*” denotes standard SL. Column “*w/ Pre-Training*” denotes pre-training with RCL then finetuning with SL. In cases with only few GT images available, RCL can improve SL performance via pre-training.

η	<i>w/o Pre-Training</i>	<i>w/ Pre-Training</i>
0	23.69	23.69
10	27.24	28.80
50	29.36	29.74
100	28.88	28.97
150	29.40	29.64
200	29.51	29.51

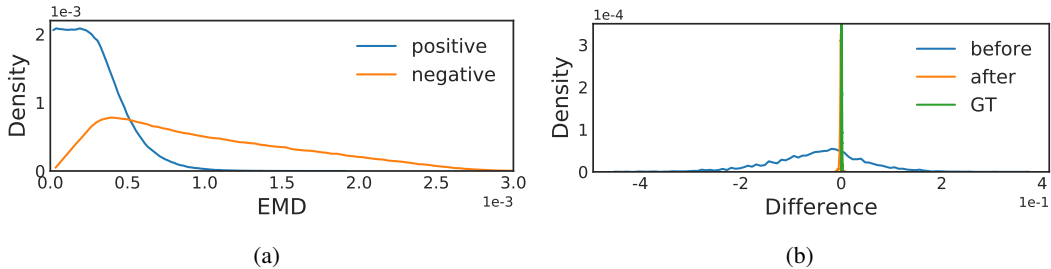


Figure 3: Density estimation plots of distributions: (a) EMD between positive pairs and EMD between negative pairs; (b) pair-wise differences of EMD between negative pairs minus EMD between positive pairs, before and after training.



Figure 4: Qualitative comparison of JDD results on a Kodak image. The noise level σ is unknown. PSNR: (b) 20.74dB; (c) 18.82dB; (d) 22.51dB; (e) 23.41dB. Best viewed in colour, with digital zoom.

Fig. 3b. We can clearly see that RCL contracts the predicted distribution closer to the true underlying distribution.

Qualitative Comparison We provide a qualitative comparison in Fig. 4 for Kodak images from Table 2, with unknown σ . Improvements are best appreciated with a digital zoom, for visualisation.

6 Limitations

The role of RCL is similar to InfoNCE in unsupervised representation learning. As a loss, RCL cannot solve JDD tasks directly. The application of RCL requires a baseline SSL JDD model to learn a coarse mapping from RAW to RGB. In addition, successful application of RCL requires a large number of high resolution RAW images. The number of independent RAW images enlarges the sample variation of the signal-dependent noise, which is essential for CL, and the high resolution can ensure large crops for accurate estimation of the statistics of the residuals. However, such conditions are not always available for practical tasks. We aim to have a quantitative analysis of RCL, thus the experiments in this study are based on Monte-Carlo simulation and the synthetic noise may differ from realistic noise. We use Gaussian noise with random σ to simulate signal-dependent noise, and concede that this does not comprehensively reflect the nature of real signal-dependent noise. Thus, the generalization of the simulated results to real RAW data remains an open question, which we consider an interesting direction for future work.

7 Conclusion

In this work, we present a principled CL strategy which can learn meaningful representations for JDD tasks from the residuals. We formulate a pretext task on RAW images for the first time and our approach leverages CL and residual learning for SSL on large-scale data. The empirical studies on the simulated signal-dependent noise not only validate the robustness of the proposed RCL, but also poses a new potential direction towards more rigorously investigating cases in which noise is unknown at test time.

References

- [1] P. Baldi and F. Pineda. Contrastive learning and neural oscillations. *Neural Computation*, 3(4):526–545, 1991.
- [2] J. Batson and L. Royer. Noise2self: Blind denoising by self-supervision. In *International Conference on Machine Learning*, pages 524–533. PMLR, 2019.
- [3] A. Bhattacharyya. On a measure of divergence between two multinomial populations. *Indian Journal of Statistics*, 7(4):401–406, 1946.
- [4] T. Chen, S. Kornblith, M. Norouzi, and G. Hinton. A simple framework for contrastive learning of visual representations. In *International Conference on Machine Learning*, pages 1597–1607. PMLR, 2020.
- [5] C.-Y. Chuang, J. Robinson, Y.-C. Lin, A. Torralba, and S. Jegelka. Debiased contrastive learning. In *Advances in Neural Information Processing Systems*, volume 33, pages 8765–8775, 2020.
- [6] K. Dabov, A. Foi, V. Katkovnik, and K. Egiazarian. Image denoising by sparse 3-d transform-domain collaborative filtering. *IEEE Transactions on Image Processing*, 16(8):2080–2095, 2007.
- [7] N. Dong, M. Xu, X. Liang, Y. Jiang, W. Dai, and E. Xing. Neural architecture search for adversarial medical image segmentation. In *International Conference on Medical Image Computing and Computer-Assisted Intervention*, pages 828–836, 2019.
- [8] T. Ehret, A. Davy, P. Arias, and G. Facciolo. Joint demosaicking and denoising by fine-tuning of bursts of raw images. In *Proceedings of the IEEE/CVF International Conference on Computer Vision*, pages 8868–8877, 2019.
- [9] M. Everingham, L. Van Gool, C. K. Williams, J. Winn, and A. Zisserman. The pascal visual object classes (voc) challenge. *International Journal of Computer Vision*, 88(2):303–338, 2010.
- [10] A. Foi, M. Trimeche, V. Katkovnik, and K. Egiazarian. Practical poissonian-gaussian noise modeling and fitting for single-image raw-data. *IEEE Transactions on Image Processing*, 17(10):1737–1754, 2008.
- [11] P. Getreuer. Color demosaicing with contour stencils. In *IEEE International Conference on Digital Signal Processing*, pages 1–6. IEEE, 2011.
- [12] M. Gharbi, G. Chaurasia, S. Paris, and F. Durand. Deep joint demosaicking and denoising. *ACM Transactions on Graphics*, 35(6):1–12, 2016.
- [13] I. J. Goodfellow, J. Pouget-Abadie, M. Mirza, B. Xu, D. Warde-Farley, S. Ozair, A. C. Courville, and Y. Bengio. Generative adversarial nets. In *Advances in Neural Information Processing Systems*, 2014.
- [14] S. Guo, Z. Yan, K. Zhang, W. Zuo, and L. Zhang. Toward convolutional blind denoising of real photographs. In *Proceedings of the IEEE/CVF Conference on Computer Vision and Pattern Recognition*, pages 1712–1722, 2019.
- [15] S. W. Hasinoff, F. Durand, and W. T. Freeman. Noise-optimal capture for high dynamic range photography. In *2010 IEEE Computer Society Conference on Computer Vision and Pattern Recognition*, pages 553–560. IEEE, 2010.
- [16] K. He, H. Fan, Y. Wu, S. Xie, and R. Girshick. Momentum contrast for unsupervised visual representation learning. In *Proceedings of the IEEE/CVF Conference on Computer Vision and Pattern Recognition*, pages 9729–9738, 2020.
- [17] K. He, X. Zhang, S. Ren, and J. Sun. Deep residual learning for image recognition. In *Proceedings of the IEEE Conference on Computer Vision and Pattern Recognition*, pages 770–778, 2016.
- [18] F. Heide, M. Steinberger, Y.-T. Tsai, M. Rouf, D. Pająk, D. Reddy, O. Gallo, J. Liu, W. Heidrich, K. Egiazarian, et al. Flexisp: A flexible camera image processing framework. *ACM Transactions on Graphics*, 33(6):1–13, 2014.
- [19] K. Hirakawa and T. W. Parks. Joint demosaicing and denoising. *IEEE Transactions on Image Processing*, 15(8):2146–2157, 2006.
- [20] R. Keys. Cubic convolution interpolation for digital image processing. *IEEE Transactions on Acoustics, Speech, and Signal Processing*, 29(6):1153–1160, 1981.
- [21] D. Khashabi, S. Nowozin, J. Jancsary, and A. W. Fitzgibbon. Joint demosaicing and denoising via learned nonparametric random fields. *IEEE Transactions on Image Processing*, 23(12):4968–4981, 2014.

- [22] D. P. Kingma and J. Ba. Adam: A method for stochastic optimization. In *International Conference on Learning Representations*, 2015.
- [23] F. Kokkinos and S. Lefkimmiatis. Deep image demosaicking using a cascade of convolutional residual denoising networks. In *Proceedings of the European Conference on Computer Vision*, pages 303–319, 2018.
- [24] A. Krull, T.-O. Buchholz, and F. Jug. Noise2void-learning denoising from single noisy images. In *Proceedings of the IEEE/CVF Conference on Computer Vision and Pattern Recognition*, pages 2129–2137, 2019.
- [25] J. Lehtinen, J. Munkberg, J. Hasselgren, S. Laine, T. Karras, M. Aittala, and T. Aila. Noise2noise: Learning image restoration without clean data. In *International Conference on Machine Learning*, pages 2965–2974. PMLR, 2018.
- [26] P. Longere, X. Zhang, P. B. Delahunt, and D. H. Brainard. Perceptual assessment of demosaicing algorithm performance. *Proceedings of the IEEE*, 90(1):123–132, 2002.
- [27] A. Majumdar. Blind denoising autoencoder. *IEEE Transactions on Neural Networks and Learning Systems*, 30(1):312–317, 2018.
- [28] H. S. Malvar, L.-w. He, and R. Cutler. High-quality linear interpolation for demosaicing of bayer-patterned color images. In *2004 IEEE International Conference on Acoustics, Speech, and Signal Processing*, volume 3, pages iii–485. IEEE, 2004.
- [29] I. Misra and L. v. d. Maaten. Self-supervised learning of pretext-invariant representations. In *Proceedings of the IEEE/CVF Conference on Computer Vision and Pattern Recognition*, pages 6707–6717, 2020.
- [30] A. v. d. Oord, Y. Li, and O. Vinyals. Representation learning with contrastive predictive coding. *arXiv preprint arXiv:1807.03748*, 2018.
- [31] O. Ronneberger, P. Fischer, and T. Brox. U-net: Convolutional networks for biomedical image segmentation. In *International Conference on Medical Image Computing and Computer-Assisted Intervention*, pages 234–241. Springer, 2015.
- [32] H. Tan, X. Zeng, S. Lai, Y. Liu, and M. Zhang. Joint demosaicing and denoising of noisy bayer images with admn. In *IEEE International Conference on Image Processing*, pages 2951–2955. IEEE, 2017.
- [33] Y. Tian, C. Sun, B. Poole, D. Krishnan, C. Schmid, and P. Isola. What makes for good views for contrastive learning. In *Advances in Neural Information Processing Systems*, volume 33, pages 6827–6839, 2020.
- [34] E. Xie, J. Ding, W. Wang, X. Zhan, H. Xu, Z. Li, and P. Luo. Detco: Unsupervised contrastive learning for object detection. *arXiv preprint arXiv:2102.04803*, 2021.
- [35] Z. Yue, H. Yong, Q. Zhao, L. Zhang, and D. Meng. Variational denoising network: Toward blind noise modeling and removal. In *Advances in Neural Information Processing Systems*, pages 1690–1701, 2019.
- [36] A. R. Zamir, A. Sax, W. Shen, L. J. Guibas, J. Malik, and S. Savarese. Taskonomy: Disentangling task transfer learning. In *Proceedings of the IEEE Conference on Computer Vision and Pattern Recognition*, pages 3712–3722, 2018.
- [37] B. Zoph and Q. V. Le. Neural architecture search with reinforcement learning. In *International Conference on Learning Representations*, 2016.

A Experiments

A.1 Bhattacharyya Distance

The *Bhattacharyya* distance (BD) has a closed-form expression if two distributions of interest are Gaussian. According to the *Central Limit Theorem*, the sample distributions of two *residual statistics vectors* are quasi-Gaussian. Formally, the BD between two Gaussian distributions $\mathcal{N}(\mu_p, \sigma_p^2)$ and $\mathcal{N}(\mu_q, \sigma_q^2)$ can be estimated as

$$d = \frac{1}{4} \ln\left(\frac{1}{4}\left(\frac{\sigma_p^2}{\sigma_q^2} + \frac{\sigma_q^2}{\sigma_p^2} + 2\right)\right) + \frac{1}{4}\left(\frac{(\mu_p - \mu_q)^2}{\sigma_p^2 + \sigma_q^2}\right), \quad (\text{A.1})$$

where μ and σ^2 are the sample mean and the sample variance. The smaller the BD is, the smaller the distributional divergence is.

A.2 Adversarial Residual Contrastive Loss

The negative distance $-d(\cdot)$ in Eq. 4 can be viewed as a similarity measure, which is analogous to $\text{sim}(\cdot)$ in Eq. 2. In this work, we want to show that $\text{sim}(\cdot)$ can also be learned in a data driven fashion. We propose to learn such a similarity measure adversarially with Eq. 4, which we term *adversarial residual contrastive loss* (ARCL). Let g_ϕ denote an auxiliary neural network, which plays a similar role to the discriminator in GANs [13]. Simply, g_ϕ takes the concatenation of two RSVs as input. The last layer of g_ϕ is a sigmoid function which makes g_ϕ output a probability score. The updated contrastive loss is

$$\mathcal{L}_{\text{adv}} = -\log \frac{\exp(g_\phi(z_q, z_0)/\tau)}{\sum_{i=0}^N \exp(g_\phi(z_q, z_i)/\tau)}. \quad (\text{A.2})$$

Note, z is extracted from $\hat{n}(x) = x - \text{mosaic}(f_\theta(x))$, which is related to f_θ , *i.e.* f_θ and g_ϕ are playing a minimax game via Eq. A.2. Eq. 5 is updated to

$$\mathcal{L}_{\text{total}} = \mathcal{L}_{\text{consistency}} + \lambda \mathcal{L}_{\text{adv}}. \quad (\text{A.3})$$

We adopt an alternative training strategy similar to [13] given the updated contrastive loss. For each mini-batch in the training process, we first maximize Eq. A.2 with f_θ fixed for k steps, then minimize Eq. A.3 with g_ϕ fixed for 1 step. Given a minibatch of $N + 1$ RAW images, the construction of the minibatch version of Eq. A.2 is similar to *SimCLR* [4]. Each RAW image generates two random crops as a positive pair. So for each anchor image x_q , there is 1 positive pair and N negative pair for Eq. A.2. The training procedure is outlined in Algorithm 1.

Considering the possible neural architectures for g_ϕ is a large finite set, it is impossible to traverse all of them empirically to get the best performance. We hypothesize that, the auxiliary network g_ϕ could be tailored by neural architecture for a given f_θ search [7] and there is still space for the performance of ARCL to be improved, which we leave to future work.

A.3 Simulation Model

We adopt a simulation model in Sec. 5.1 to validate the theoretical results of learning from residuals. We assume a uniform distribution $\mathcal{U}(0, 20)$ to sample σ for each RAW image. In practice, for real images, the distribution for σ is not necessarily uniform, and it could be more complex than the simulated study we have in this work. We choose this simplified simulation model for an initial understanding of RCL and for a controllable comparison with other baseline methods.

Intuitively, RCL should benefit from a large variation of σ , which makes two negative pairs dissimilar. Here, we evaluate a different noise simulation model with σ sampled from $\mathcal{U}(0, 10)$. The PSNR results are shown in Table A.1. We report the mean and standard deviation of the PSNR for 5 different random seeds and the network backbone is U-Net [31].

Ideally, given a smaller σ on average, PSNR should be higher. However, as shown in Table A.1, $\mathcal{U}(0, 10)$ does not improve the performance significantly. We hypothesize that RCL is not in favor of a small variation of instance-wise noise distribution, considering that there is a smaller variation of σ sampled in $\mathcal{U}(0, 10)$ than σ sampled in $\mathcal{U}(0, 20)$.

Algorithm 1: Minibatch stochastic gradient descent training of ARCL. The number of steps to apply to g_ϕ , k is a hyperparameter. Empirically, we find that $k = 5$ gives the best performance.

- Initialize f_θ, g_ϕ .

for number of training iterations **do**

for k steps **do**

- Sample minibatch of $N + 1$ RAW images.
- Update g_ϕ by ascending its stochastic gradient:

$$\nabla_\phi \frac{1}{N + 1} \sum_{q=0}^N \mathcal{L}_{\text{adv}}.$$

end

- Sample minibatch of $N + 1$ RAW images.
- Update f_θ by descending its stochastic gradient:

$$\nabla_\theta \frac{1}{N + 1} \sum_{q=0}^N \mathcal{L}_{\text{total}}.$$

end

Table A.1: PSNR results for RCL with different noise simulation model. The σ is random (unknown) when we generate synthetic signal-dependent noise. The U-Net backbone is initialized with different random seeds for 5 times.

σ	MIT	Stanford	VOC
$\mathcal{U}(0, 10)$	28.29 ± 0.47	27.04 ± 0.54	23.13 ± 0.44
$\mathcal{U}(0, 20)$	28.12 ± 0.25	26.95 ± 0.38	23.17 ± 0.21

A.4 Robustness of Residual Contrastive Loss

We examine the robustness of the proposed framework by reporting the error bars in Table A.2. Given the same U-Net initialized with different random seeds for 5 times, we report the mean and standard deviation of the PSNR results for RCL with EMD, RCL with BD, and ARCL on MIT, Stanford, and VOC datasets respectively. All variants of RCL are robust against random seed. Among three variants of RCL, RCL with EMD has the best overall performance by considering both mean and standard deviation. RCL with BD has the smallest standard deviation and ARCL has the highest standard deviation.

A.5 Implementation

We implement *bilinear interpolation* [26] and *noise2self* [2] (with a U-Net [31] backbone) by PyTorch. We implement the proposed framework by PyTorch, where the choice of hyperparameters follows the source code of *mosaic2mosaic* [8], *MoCo* [16], *SimCLR* [4], and *GAN* [13] respectively.

Table A.2: PSNR results for RCL with the error bars. The σ is random (unknown) when we generate synthetic signal-dependent noise. The U-Net backbone is initialized with different random seeds for 5 times.

Method	MIT	Stanford	VOC
RCL (BD)	27.71 ± 0.24	26.66 ± 0.25	23.02 ± 0.12
RCL (EMD)	28.12 ± 0.25	26.95 ± 0.38	23.17 ± 0.21
ARCL	25.90 ± 0.54	25.77 ± 0.53	21.73 ± 0.26

B Additional Visualizations

We provide additional visualizations for MIT, Stanford, and VOC datasets in Fig. B.1, Fig. B.2, and Fig. B.3 respectively. When the noise level is small (*e.g.* the third row in Fig. B.3), all methods have similar performance. When the noise level is too high (*e.g.* the second row in Fig. B.1 and the second row in Fig. B.2), all methods almost fail.

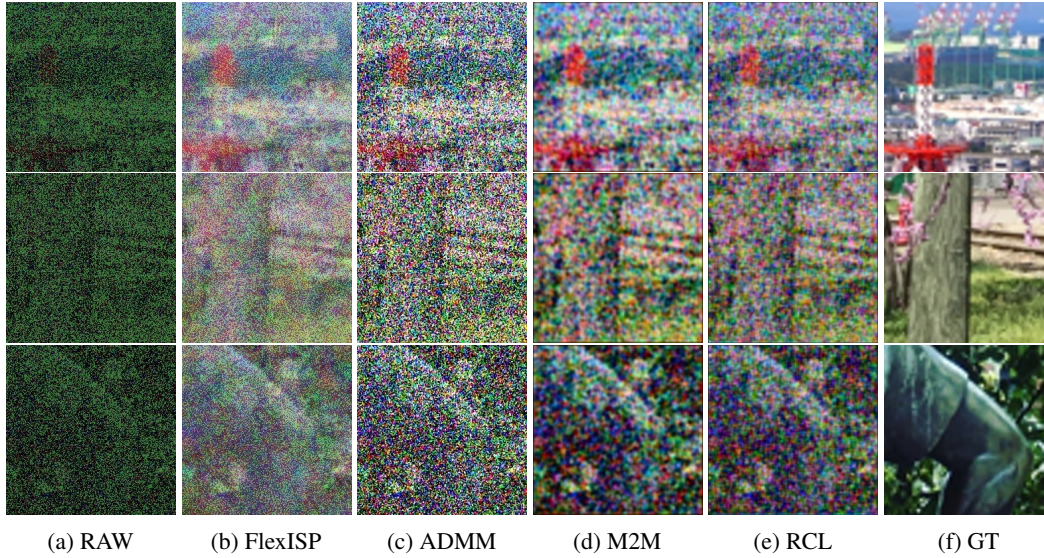


Figure B.1: Qualitative comparison of JDD results on MIT dataset. σ is randomly sampled from $\mathcal{U}(0, 20)$.

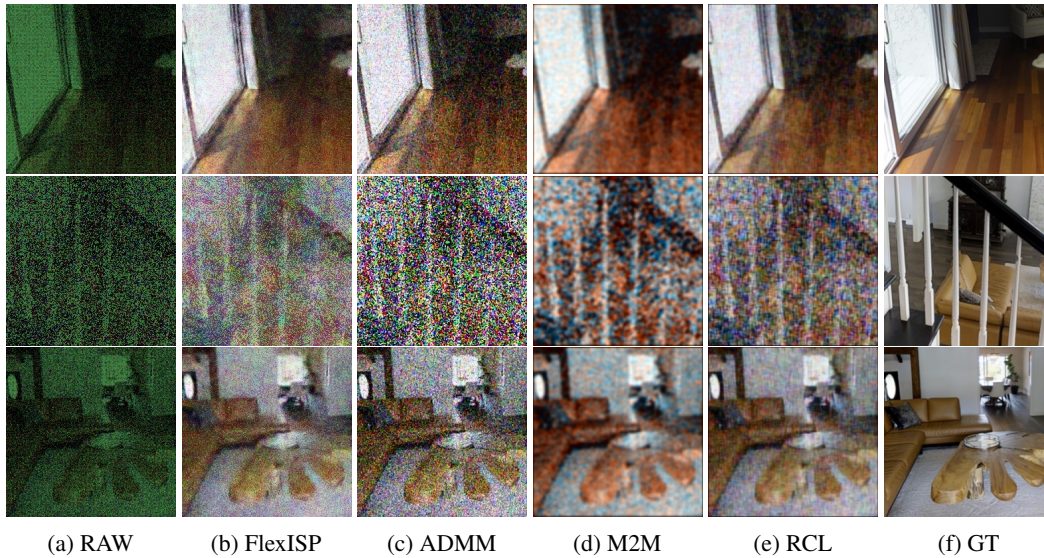


Figure B.2: Qualitative comparison of JDD results on Stanford dataset. σ is randomly sampled from $\mathcal{U}(0, 20)$.

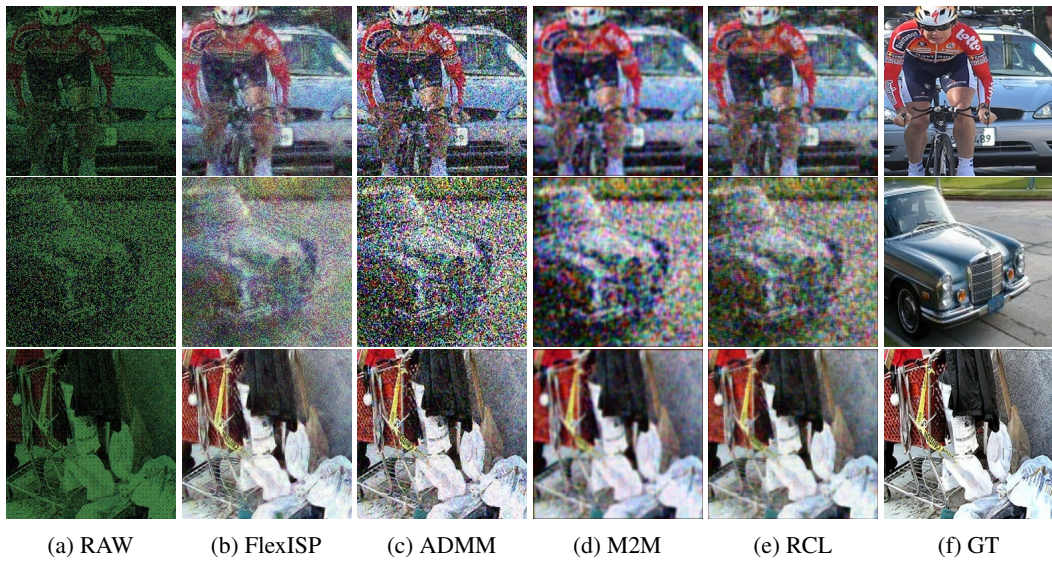


Figure B.3: Qualitative comparison of JDD results on VOC dataset. σ is randomly sampled from $\mathcal{U}(0, 20)$.